Journal of Power Sources 190 (2009) 110–120

Contents lists available at ScienceDirect

Journal of Power Sources

journal homepage: www.elsevier.com/locate/jpowsour

Characterization of water transport in gas diffusion media

Christian Quick[a,*], Dietrich Ritzinger[a], Werner Lehnert[b], Christoph Hartnig[b]

[a] Freudenberg Fuel Cell Component Technology KG, D-69465 Weinheim, Germany
[b] Centre for Solar Energy and Hydrogen Research, D-89081 Ulm, Germany

ARTICLE INFO

Article history:
Received 3 June 2008
Received in revised form 28 July 2008
Accepted 31 July 2008
Available online 19 August 2008

Keywords:
PEM fuel cell
Gas diffusion layer
Water management
Water transport

ABSTRACT

An in-depth insight in the role of gas diffusion layers (GDLs) and its impact on the water management is a key issue for the optimization of fuel cells. A new *ex situ* test method is developed to investigate the water transport in gas diffusion media for polymer electrolyte membrane fuel cells (PEMFCs). This research is focused on properties of GDLs, which influence the water removal and water retention in the cell.

Gas diffusion media are evaluated *ex situ* in terms of liquid water and water vapor transport employing a conventional PEMFC setup. The amount of water transported through a GDL and out of the cell is determined by the properties of the gas diffusion medium. GDL properties such as the GDL thickness have a significant impact on water transport behavior. Furthermore, high impregnation weight or an additional micro-porous layer (MPL) reduces water removal due to enhanced mass transport resistances. The composition and distribution of the impregnation material in the GDL substrate also play a crucial role. Water transport rates depend not only on the GDL properties but increase exponentially with cell temperature.

Finally, a two-phase water transport model is proposed taking into account both diffusive gas phase and liquid water transport in diffusion media. Based on this model, *ex situ* data set in correlation with *in situ* performance in PEMFCs on dry operating conditions and guidelines towards new design concepts for gas diffusion media are deduced.

1. Introduction

Water management plays an important role for a high performance and efficient operation of PEMFCs [1–3]. On the one hand, the polymer electrolyte membrane has to be hydrated sufficiently to ensure a good proton conductivity, which increases with increased water content [4]. Water is produced at the cathodic catalyst layer (CL) in the electrochemical reaction. Additionally, the reactant gases can be humidified. On the other hand, the active surface of the CL as well as pores in the GDL can be flooded by excessive liquid water, resulting in a higher mass transport resistance [5–7]. The consequence is oxygen transport limitation at the active layer that finally lowers fuel cell performance. Regarding this conflicting role of water, a delicate balance is required. So far, no generally applicable strategy for optimal water management in PEMFCs is available because water transport in the different components of a fuel cell is influenced by operating conditions like humidification level of the reactant stream, reactant stoichiometric ratio as well as the temperature and pressure of the cell. Furthermore the geometric characteristics of the flow field and the physical characteristics of the membrane and the GDL have a strong impact on the water transport [8].

Among the PEMFC components, the GDL plays a crucial role for a high performance because the diffusion media has lots of important tasks in the fuel cell. On the one hand the reactant gases have to be distributed homogeneously from the flow field to the CL for the electrochemical reaction. On the other hand the GDL should remove heat and excess water from the electrode to prevent local hotspots and catalyst flooding. Further the diffusion medium represents a mechanical reinforcement for the mechanically sensitive catalyst-coated membrane (CCM) [9,10]. The required properties of a GDL are therefore good electrical and thermal conductivity as well as high thermal and chemical resistance and enhanced water and gas permeability. However, some of these requirements are contradictive. For example, air and water permeability increase with higher porosity, contrary to mechanical properties, electrical and thermal conductivity. Additionally all these mentioned characteristics are influenced by the GDL thickness, hydrophobicity and alignment of the carbon fibers. For further information Mathias et al. gave a comprehensive overview of GDL structure and functions [9].

Abbreviations: atm, atmosphere (ambient pressure); CB, carbon black; CCM, catalyst-coated membrane; CL, catalyst layer; FEP, fluorinated ethylene propylene copolymer; GDL, gas diffusion layer; ip, in-plane direction; MEA, membrane electrode assembly; MPL, micro-porous layer; PEMFC, polymer electrolyte membrane fuel cell; PTFE, polytetrafluoroethylene; tp, through-plane direction; wt, weight.

* Corresponding author. Tel.: +49 6201 80 2289; fax: +49 6201 88 2289.
E-mail address: christian.quick@freudenberg.de (C. Quick).

0378-7753/$ – see front matter © 2008 Elsevier B.V. All rights reserved.
doi:10.1016/j.jpowsour.2008.07.093

Nomenclature

A	area (m^2)
c	concentration ($mol\,l^{-1}$)
d	thickness (m)
d_p	pore diameter (m)
dp	differential pressure (Pa)
D	binary diffusion coefficient in air ($m^2\,s^{-1}$)
f	geometrical factor for increased diffusion distance
F	Faraday constant ($C\,mol^{-1}$)
H	enthalpy ($J\,mol^{-1}$)
J	current density ($A\,m^{-2}$)
K	gas permeability ($l\,s^{-1}\,m^{-2}$)
m	weight (g)
$\dot{m}$	mass flow ($g\,s^{-1}$)
M	molecular weight ($g\,mol^{-1}$)
n	mole (mol)
$\dot{n}$	mole flow ($mol\,s^{-1}$)
p	pressure (Pa)
p_c	capillary pressure (Pa)
Δp	pressure drop (Pa)
R	constant factor for ideal gases ($J\,mol^{-1}\,K^{-1}$)
t	time (s)
T	temperature (T)
$\dot{V}$	volume flow ($ccm\,min^{-1}$ = sccm)
WT	water transport rate ($mg\,min^{-1}$)
Y	loading of humidified air

Greek symbols

θ_c	contact angle (°)
ν	atomic diffusion volume
σ	surface tension ($N\,m^{-1}$)
φ	relative humidity

Subscripts/superscripts

eff	effective
equiv	equivalent
exp	experimental
g	gas phase
H_2O	water
max	maximum
mol	amount of substance
out	outlet
sat	saturation
theo	theoretical
vap	vapor
0	standard conditions (273.15 K, 101,325 Pa)

In general, there are three main types of carbon fiber substrates which are employed as a gas diffusion layer (GDL): carbon paper [11,12], carbon cloth [11,13,14] and carbon non-woven [15]. Expanded or sintered metals are also used for some applications [4]. Contrary to paper and non-woven, cloth is a woven material, which has right-angled crossed threads of, carbonized bundles of wool or synthetic fibers, thus no binder is needed. Due to these differences in carbon fiber structure as well as the resulting different physical properties between cloth and paper, experimental studies indicate varying *in situ* performances of PEMFCs of both substrates [16–18]. Ralph et al. showed that the carbon cloth performs better than the carbon paper on fully humidified conditions owing to an efficient water removal [16]. Contrary, carbon paper indicates higher fuel cell performance on dry operating conditions, probably due to better water retention behavior. In this work, only carbon paper and carbon non-woven were investigated and compared.

In order to prevent flooding of the CL, gas diffusion media are commonly treated with a hydrophobic agent such as PTFE [9,19–21]. Thus, most of the water, especially the product water at the cathode of the PEMFC, can be efficiently removed from the active layer through the GDL to the flow field channels. Such a treatment leads to a mixture of hydrophilic and hydrophobic pores in the GDL [9,22] and hence, inhibits water condensation in the GDL pores completely and ensures a low water saturation level, respectively [19]. Atiyeh et al. assumed that hydrophobic regions allow a pathway for gas transport whereas the hydrophilic parts facilitate liquid water transport [23]. Consequently, the improved water management is able to reduce mass transport resistance and enhance fuel cell performance [19]. The effect of PTFE content on PEMFC performance has been extensively studied in many studies [18,24,25]. Increasing the PTFE loading leads to higher hydrophobicity, but lowers the electrical conductivity at the same time [11]. Additionally, porosity of the GDL is also reduced resulting in higher mass transport resistance [11,15,26]. However, insufficient water removal capability occurs at too low PTFE content. Presumably owing to PTFE degradation in the GDL after long-term operation, poor water management takes effect leading to a rapid degradation of the membrane electrode assembly (MEA) [25,27]. Therefore, a GDL plays an important role concerning the durability of the MEA. In the end an optimal amount of PTFE must be determined experimentally regarding to the operating conditions of the fuel cell [26]. Optimum PTFE content in the range of 10–30% is reported [19,28–31].

Quite often the GDL possesses a double layer structure [18,25,28,32,33]. The main part of the GDL is the macro-porous carbon fiber substrate. The second layer is a thinner micro-porous layer (MPL) consisting of a mixture of carbon black (CB) and a hydrophobic agent [9]. It is able to improve gas diffusion and water management due to suitable surface pore size [26,28,33,34] and hydrophobicity to prevent flooding of the electrode and to minimize electronic contact resistance with the adjacent CL. The additional layer also acts as a protection of the thin CCM from carbon fibers of the GDL substrate [30]. The typical MPL pore diameter is in the range of 0.02–0.5 μm [32] compared to that of the GDL, which is between 1 μm and 100 μm [9,23,35]. According to the assumption that water condensation occurs hardly in hydrophobic pores smaller than 1 μm, GDLs with an additional MPL have lower water saturation level resulting in higher gas transport at the CL [26,36]. Some studies supposed that, depending on several characteristics like hydrophobicity, thickness, pore diameter and porosity, the MPL is able to block liquid water at the interface to the cathodic CL and supports back diffusion through the membrane to the anode [26,32,37–39]. Thus, Pasaogullari et al. indicated that the strong capillary pressure in the MPL retains a higher-pressure gradient across the CCM which in turn favors the water transport from the cathode to the anode [39]. On the other hand it was also reported that the MPL provides effective wicking of liquid water from the active layer into diffusion media and finally to the flow field channels [9,30,36,40]. However, this effect will only occur if there is a hydrophilic pore-network for capillary transport of liquid water [41]. All those studies clearly point out contrasting explanation on the role of MPL on the water management. Despite these rather contrary interpretations on MPL functions, it has been reported that an additional MPL coating can significantly enhance fuel cell performance [26,28,33,34,38].

So far there have been many attempts to improve fuel cell performance by developing or modifying gas diffusion media. Most studies observed enhanced performance after a single treatment process on the GDL. However, it is difficult to identify the result-

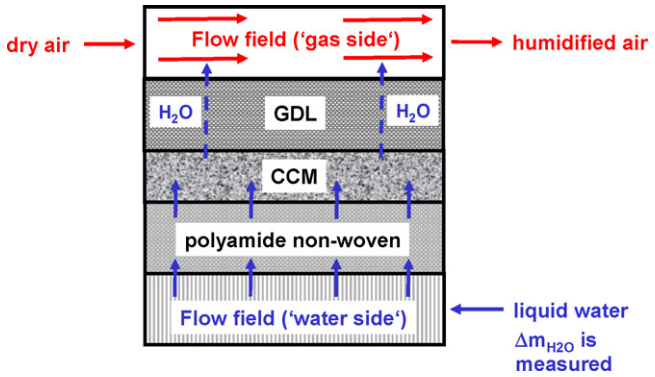

Fig. 1. Sketch of the modified PEMFC for *ex situ* water transport measurement.

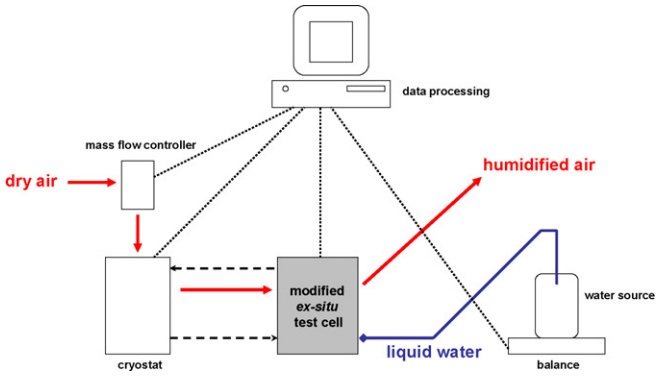

Fig. 2. Schematic representation of the experimental setup.

ing material properties that affect the fuel cell performance most, speculated are mechanical or electrical properties on the one hand or mass and heat transport on the other hand. In this study, the focus was set on the properties of GDLs, which influence the water transport behavior. By means of a suitable *ex situ* test method a fast screening of GDL samples should reduce the number of time-consuming and cost-intensive *in situ* cell tests. Furthermore, new design concepts for tailor-made gas diffusion media could be given from a simplified approach. Previously, Wang et al. investigated factors that have impact on mass and heat transfer in a porous media plate [42]. Cell temperature, air flow velocity as well as the thickness, pore diameter, hydrophobicity and previous vacuum impregnation of the porous material affect the mass transport.

2. Experimental

2.1. Principle of measurement

Fig. 1 shows the setup of the water transport measurement: The GDL separates a saturated phase with liquid water ('water side') from a gas phase ('gas side') and the water transport rate through the diffusion media was determined as function of the air flow at the 'gas side'. The assumption was made that differences in the water removal properties are due to different crucial properties of the investigated GDLs.

2.2. Apparatus

A modified, horizontally orientated fuel cell was used for the experiment. The 'water side' and the 'gas side' were separated from each other with a conventional catalyst-coated polymer electrolyte membrane of the *Primea® Series 5510* from *W.L. Gore&Associates Inc.* (*USA*, *MD*)[1]. Certain trade names and company products are mentioned in the text or identified in an illustration are in order to adequately specify the experimental procedure and equipment used. In no case does such an identification imply recommendation or endorsement nor does it imply that these materials are necessarily the best available for the application.

The pure membrane without the CLs is 35 μm thick with an active area of 50 cm^2. The assumption was made that no mass transport limitation occurred by the CCM, i.e. the membrane was always fully saturated with liquid water. At the 'gas side' of the cell, a counter-flow of dry air passed through a straight channel flow field. The geometry of the graphite 'gas side' flow field was optimized to achieve homogeneous gas distribution and to minimize pressure drop (<6000 Pa) in the flow channels. The preheated air flow was varied in the range of 100–15,000 sccm to transport water out of the cell. The investigated GDL was positioned between the 'gas side' flow field and the CCM. At the 'water side', a hydrophilic polyamide non-woven which soaked up the liquid water was placed between the CCM and a graphite one-channel serpentine flow field. A connecting tube between the test cell and a water source provided the serpentine flow field on the 'water side' with sufficient liquid water. The water container was placed on a balance. During the experiment the water loss in the reservoir was recorded and corresponded to the amount of water removed at the 'gas side' of the cell. The measurement was performed at a constant temperature of 54.5 °C, a cell compression of 0.6 MPa and an ambient pressure at the cell outlet of the 'gas side'. To ensure isothermal conditions during measurement, a cryostat was employed. Fig. 1 illustrates the modified *ex situ* test cell and Fig. 2 depicts the complete measurement setup. Additionally, Table 1 compiles the respective operation parameters.

2.3. Materials

Dry-laid non-woven based GDLs were investigated in this study and were manufactured and treated in-house by Freudenberg. All non-wovens based on the identical GDL substrate with the same carbon fiber density differing from each other just by the hydrophobic treatment. The naming of the investigated materials depends on the type of substrate (NW = carbon fiber non-woven), the kind of impregnation (*I* = impregnated by a CB/PTFE mixture, *T* = teflonated by pure PTFE) as well as the use of a MPL (*C*). Concerning the treatment of the GDL substrate, the first number describes the impregnation weight whereas the second value is the percentage of PTFE. Further teflonated materials are denoted by adding "*i*" and "*h*", respectively. "*i*" states an inhomogeneous PTFE distribution while the latter expresses a more homogeneously distributed hydrophobic agent. All materials used in this study, except NW T10h, NW T20h, NW T30h and NW T40h, were dried by means of a convective drying process. The latter were treated by a diffusive drying

Table 1
Operation parameters of the *ex situ* water transport measurement

T_{cell}	54.5 °C (isothermal)
p_{out}	Ambient pressure
$p_{cell\ compression}$	0.6 MPa
A_{cell}	50 cm^2
$\dot{V}_{air}$	100–15,000 sccm

[1] Certain trade names and company products are mentioned in the text or identified in an illustration are in order to adequately specify the experimental procedure and equipment used. In no case does such an identification imply recommendation or endorsement nor does it imply that these materials are necessarily the best available for the application.

Table 2
Investigated gas diffusion media with *ex situ* data; NW = carbon fiber non-woven, *T* = teflonated by pure PTFE, *I* = impregnated by a carbon black/PTFE mixture, *C* = micro-porous layer coating, *i* = inhomogeneous PTFE distribution, *h* = more homogeneous PTFE distribution, sample 5: (2) means the second lot of this GDL type

Sample	GDL	Impregnation weight (wt.%)	Carbon black/PTFE	MPL	WT (mg min^{-1})	tp gas permeability (μm^2)[a]
1	NW T0	0	–	–	599	6.972
2	NW0 T0	0	–	–	636	11.503
3	NW1 T0	0	–	–	545	6.607
4	NW T10i	10	0/100	–	561[b] (567)	7.424
5	NW T10i(2)	10	0/100	–	569	6.579
6	NW T10h	10	0/100	–	585[b]	9.059
7	NW T20i	20	0/100	–	545[b]	6.854
8	NW T20h	20	0/100	–	575[b]	6.966
9	NW T30i	30	0/100	–	530[b] (495)	5.961
10	NW T30h	30	0/100	–	557[b]	6.027
11	NW T40i	40	0/100	–	508[b]	4.675
12	NW T40h	40	0/100	–	544[b]	5.053
13	NW I20-20	20	80/20	–	518[b]	2.570
14	NW I20-40	20	60/40	–	535[b] (529)	3.846
15	NW I20-60	20	40/60	–	555[b]	4.951
16	NW I20-80	20	20/80	–	576[b]	6.265
17	NW I05-20	5	20/80	–	562[b]	7.352
18	NW I10-40	10	60/40	–	538[b]	5.497
19	NW I10-60	10	40/60	–	582	5.904
20	NW I30-60	30	40/60	–	487	0.671
21	NW I35-10	35	90/10	–	465[b]	0.509
22	NW T0 C2	0	–	C2	494	0.049
23	NW T10 C1	10	0/100	C1	500	0.104
24	NW T10 C3	10	0/100	C3	449	0.011
25	NW I20-40 C1	20	60/40	C1	445	0.071
26	NW I20-40 C3	20	60/40	C3	416	0.010

[a] Determined according to EN ISO 9237 at 200 Pa.
[b] Water transport is normalized to a GDL thickness of 185 μm.

procedure. Relating to the MPL-coating the same CB, binder and composition were used for the C1- and the C3-MPL whereas the latter points out a lower through-plane (tp) gas permeability due to minor density. In contrast to C1 and C3, the C2-coating was manufactured with another type of binder but have the same CB and coating composition. Table 2 contains details of all examined diffusion media and relevant physical parameters such as water transport rate and tp gas permeability.

2.4. Data processing

The weight of the water source, the pressure drop in the 'gas side' flow field as well as the air flow rate and the cell temperature were measured as function of time. At first, the air flow was varied in a wide range of 100–15,000 sccm to estimate the influence of the GDL on the water transport. Each measurement was repeated two times and the average value was calculated. The repeatability of the measurement was ensured owing to a maximum error of just 2%. In Fig. 3 the typical data distribution is presented.

Air and water vapor were considered as ideal gases to simplify the analysis:

$$p\dot{V} = \dot{n}RT \tag{1}$$

The mass flow of the dry air ('gas side') is calculated using $\dot{n}_{air} = \dot{m}_{air}/M_{air}$:

$$\dot{m}_{air} = \frac{p_0 \dot{V}_{air} M_{air}}{RT_{cell}} \tag{2}$$

With help of relation (3), the theoretical mass water flow can be calculated:

$$\dot{m}^{theo}_{H_2O} = Y\dot{m}_{air} \tag{3}$$

where Y is the loading of the humidified air:

$$Y = \frac{\varphi p^{sat}_{H_2O}}{p_{cell} - \varphi p^{sat}_{H_2O}} \frac{M_{H_2O}}{M_{air}} \tag{4}$$

If a completely saturated air flow is assumed, the relative saturation will be $\varphi = p_{H_2O}/p^{sat}_{H_2O} = 1$ and Eq. (5) is able to be derived from (4):

$$Y = \frac{p_{H_2O}}{p_{cell} - p_{H_2O}} \frac{M_{H_2O}}{M_{air}} \tag{5}$$

Combining Eq. (3) with (2) and (5) leads to the final expressions (6):

$$\dot{m}^{theo}_{H_2O} = Y\dot{m}_{air} = \frac{p_{H_2O}}{p_{cell} - p_{H_2O}} M_{H_2O} \frac{p_0 \dot{V}_{air}}{RT_{cell}} \tag{6}$$

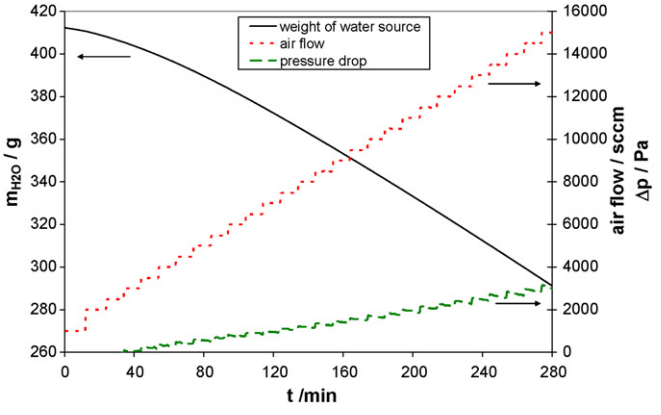

Fig. 3. Raw data of the *ex situ* water transport measurement: weight of the water source, pressure drop, air flow, cell temperature (54.5 °C, atm, 50 cm^2).

The partial pressure of water vapor is determined using the Antoine equation:

$$p_{H_2O} = 100 \exp\left(A - \frac{B}{T_{cell} + C}\right) \quad (7)$$

Relation (7) is valid for temperatures in the range between 0.11 °C and 70 °C at atmospheric pressure where A, B and C are constant parameters which amount to 19.016, 4064.95 and 236.25, respectively [43].

3. Results

Fig. 4 presents the water transport of three different GDLs as function of the air flow rate: water flow through the porous media increases with increasing air stream. At higher gas stream significant differences between the water flow rates were observed. Hence, different types of gas diffusion media can be classified regarding their treatment and the resulting properties. Accordingly, these results prove the suitability of our new test method. Fig. 4 also indicates the comparison between the experimental water transport rate through the GDLs and the theoretical water flow, which would be possible, when air flow is 100% humidified according to Eq. (6). The higher the air flow rate, the lower the relative humidity of the air stream that leaves the test cell at the 'gas side'. At flow rates between 12,000 sccm and 15,000 sccm the water transport shows saturation and the maximum water removal (transport rate) was employed for further evaluation. Using the experimental water transport data the equivalent current density can be determined:

$$J_{equiv}^{exp} = \frac{2F\dot{m}_{H_2O}^{exp}}{M_{H_2O}A_{cell}} \quad (8)$$

The corresponding values are illustrated in Fig. 4, too. The equivalent current density indicates the maximum of product water which is capable to be removed in a corresponding *in situ* cell by the given air flow.

In Fig. 5 the water transport behavior of three untreated raw materials with different thicknesses is displayed. The maximum water flow appears to decrease linearly with increasing GDL thickness. The increased diffusion pathways through the thicker diffusion media is the most reasonable explanation for this behavior. Hence, the data of all investigated non-woven GDLs without a MPL-coating were normalized to a fixed thickness of 185 μm for comparison purposes.

Fig. 6 compares various substrates with and without a MPL regarding water transport and tp gas permeability, respectively. An additional layer leads to a higher mass transport resistance lowering the water removal through the GDL. The water flow depends not only on the presence of the MPL but on the MPL properties as well. Hence, the denser C3-coating results in lower water transport due to higher mass transport resistance.

In order to investigate the effects of the GDL treatment on the water transport one has to differentiate between the content and the composition of the impregnation (see Fig. 7). Two different approaches were chosen: in the first step, the PTFE content was kept constant at 4 wt.% varying the total loading. At second, the absolute content was kept constant at 20 wt.% with varying PTFE content as optimum loadings in the range of 10–30 wt.% have been reported [19,28–30]. The scheme of both studies is outlined in Fig. 7.

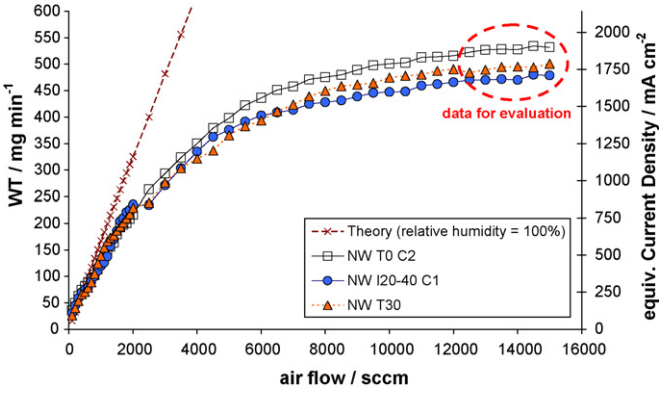

Fig. 4. Water transport (WT) and the equivalent current density as function of air flow for different gas diffusion media (54.5 °C, atm, 50 cm²).

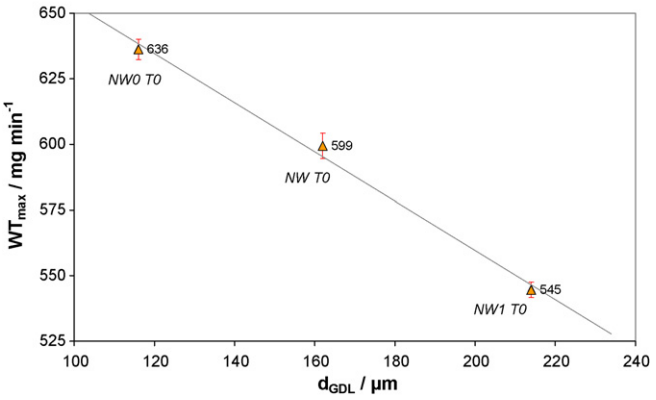

Fig. 5. Water transport (WT) as function of the GDL thickness; NW0 is thinner and NW1 thicker than the standard GDL substrate NW (54.5 °C, atm, 15,000 sccm, 50 cm²).

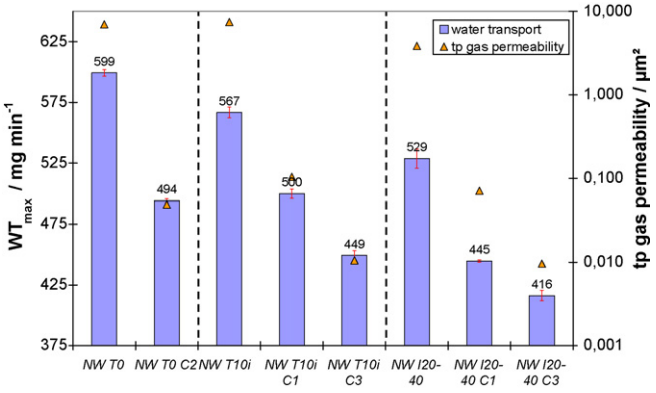

Fig. 6. Impact of the micro-porous layer (MPL) on the water transport rate (WT) (54.5 °C, atm, 15,000 sccm, 50 cm²).

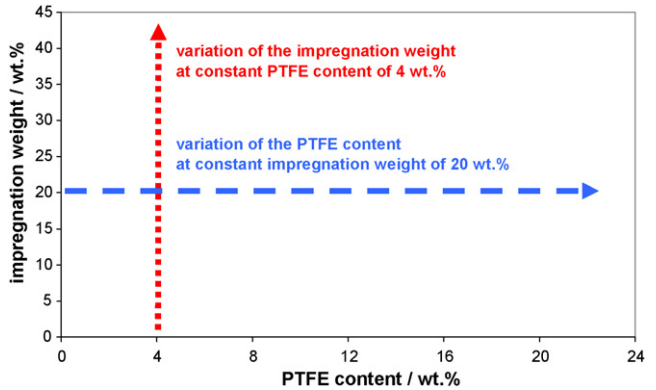

Fig. 7. Schematic presentation of the parameter variations.

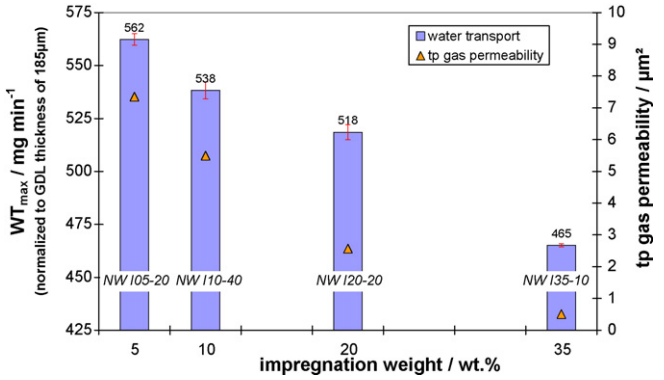

Fig. 8. Dependence of the water transport (WT) and through-plane gas permeability on the impregnation weight at a constant PTFE content of 4 wt.% (54.5 °C, atm, 15,000 sccm, 50 cm^2).

Fig. 8 presents the impact of the impregnation weight variation on water transport. A linear correlation between the water transport rate and the weight of treatment can be noticed. The higher the amount of impregnation, the smaller the porosity, the lower is the water flow in the GDL owing to higher mass transport resistance. Moreover, the water transport rate is also correlated to the tp gas permeability in Fig. 9. The water flow indicates a linear relation with increasing gas permeability. In the second study the impact of the composition of the impregnation mixture was investigated while keeping the total impregnation weight constant. In Fig. 10 the water transport is plotted to the absolute PTFE loading at a constant treatment weight of 20 wt.% of a CB/PTFE composition. The materials point to a linear relation of the water flow with increasing PTFE content. A maximum of water transport is achieved at 16 wt.% PTFE (CB/PTFE = 20/80) after which water flow drops for pure PTFE impregnation (full colored columns).

The impact of pure PTFE loading on the water transport was analyzed by means of homogeneous as well as inhomogeneous PTFE distribution. A linear decay of the maximum water flow by increasing the PTFE loading for both types of distribution is observed in Fig. 11. Actually, the water transport rates of the samples which were dried by means of a slow diffusive process (homogeneous) always show significant higher water transport than the convectively (inhomogeneous) dried materials.

Finally, the effect of the cell temperature was examined for two different materials in order to estimate the contribution of single or two-phase flow phenomena. The exponential correlation between the temperature and the water transport rate is presented in Fig. 12.

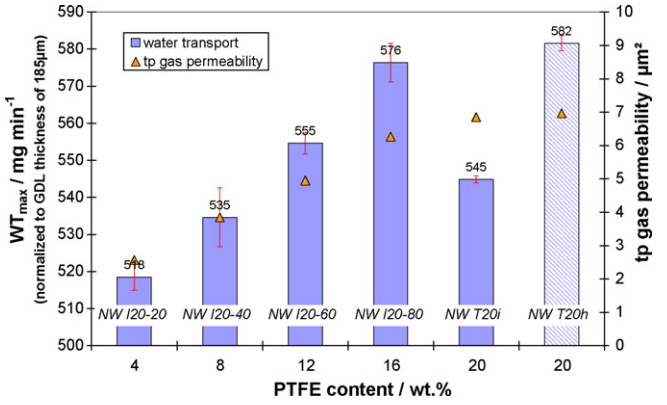

Fig. 10. Water transport (WT) and through-plane gas permeability as function of the absolute PTFE content at a constant impregnation weight of 20 wt.% (colored columns) and a more homogeneous PTFE distribution at 20 wt.% (striped column) (54.5 °C, atm, 15,000 sccm, 50 cm^2).

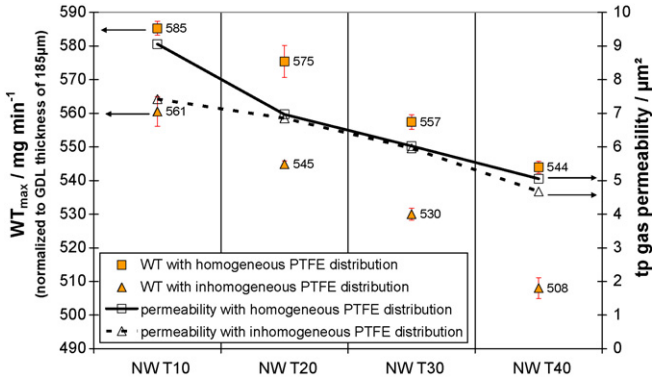

Fig. 11. Water transport (WT) of GDLs with different PTFE loading and distribution (54.5 °C, atm, 15,000 sccm, 50 cm^2).

In the present study the *ex situ* test method introduced by Baker et al. is implemented to correlate water transport data with the relative effective diffusivity in tp direction [44]. Uncompressed GDLs were used for the diffusion experiments whereas the GDLs were compressed at 0.6 MPa for the water transport examination of this publication. This slight distinction, however, do not affect the overall trend. The correlation between water transport and relative diffusivity is illustrated in Fig. 13.

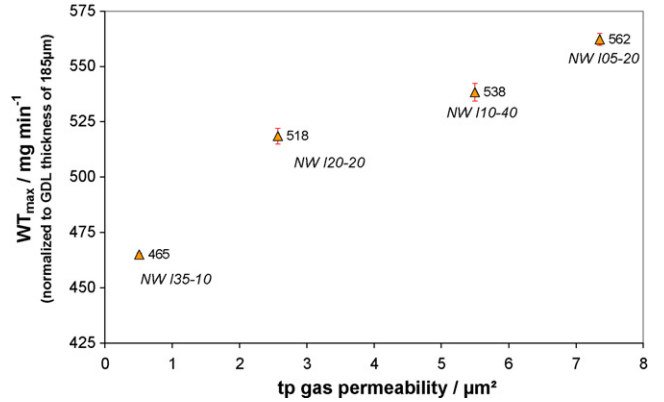

Fig. 9. Correlation of water transport (WT) with through-plane gas permeability (54.5 °C, atm, 15,000 sccm, 50 cm^2).

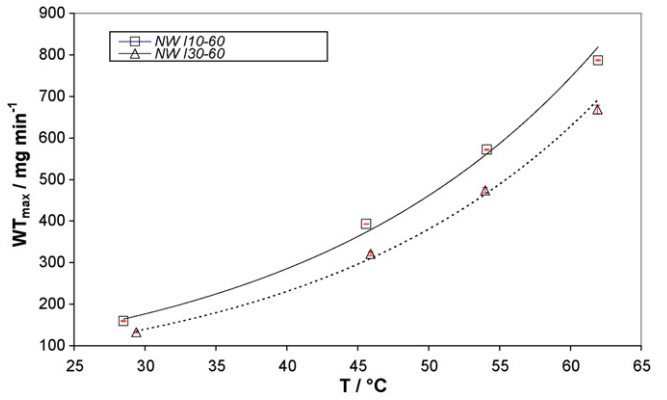

Fig. 12. Water transport (WT) as function of the cell temperature for two different materials (atm, 15,000 sccm, 50 cm^2).

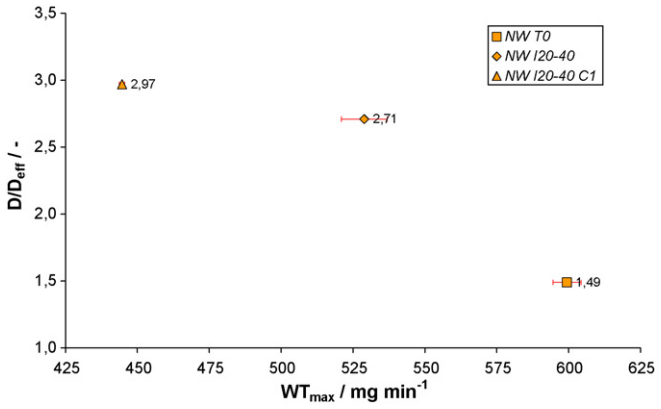

Fig. 13. Correlation between relative effective through-plane diffusivity and water transport (WT) of several gas diffusion media (54.5 °C, atm, 15,000 sccm, 50 cm^2).

4. Discussion

4.1. Impact of GDL thickness

In Fig. 5 the linear decrease of water transport with enhanced GDL thickness can be explained by the increased diffusion pathways through the thicker diffusion medium. Several studies reported that a thinner gas diffusion medium shortens the path length of mass transfer resulting in a minor transport resistance. Accordingly, the concentration gradient becomes larger, which in turns facilitates the mass transport through the material [42,45–47].

4.2. Impact of MPL-coating

As it can be seen in Fig. 6 an additional MPL coated on GDLs causes an enhanced mass transport resistance due to the smaller pore sizes of the MPL. Consequently, the tp gas permeability as well as the water transport rate of the coated GDL decreases. The latter one is reduced by not more than 20% whereas the tp gas permeability drops off by two orders of magnitudes and more. Lin et al. assumed a reduced permeability of liquid water through the diffusion media owing to the small hydrophobic pores of the MPL [12]. Other observations described a blocking of the diffusion pathways caused by MPL penetrating into the GDL substrate [48]. Besides the mere presence of a MPL the water transport also depends on the properties of the additional layer. The denser C3-coating indicates a lower water transport due to higher mass transport resistance. The reduced tp permeability of the C3-coating compared to the C1-MPL emphasizes this assumption. Therefore a correlation between both water transport and tp gas permeability is presumed as well.

4.3. Impact of impregnation weight

Fig. 8 points out a linear correlation between the water transport and the weight of treatment. Higher impregnation loading results in a lower water flow in the GDL due to higher mass transport resistance. This assumption can be underlined by means of considering the linear decay of the tp gas permeability with increasing impregnation weight in the same graph. In addition, the mass transport through the GDL is improved by increasing the porosity and permeability [40,42,47]. Moreover, the direct correlation of water transport with the tp gas permeability is shown in Fig. 9 and reveals a linear enhancement of water removal with increasing tp gas permeability. As a consequence gas transport should play an important role in this measurement. Though the gas permeability is determined by using convective flow (EN ISO 9237), while diffusive transport dominates in tp direction of the diffusion media, Mueller et al. found that GDL performance in a PEMFC correlates with gas permeability where an enhanced permeability improves oxygen utilization in the limiting current region [49].

4.4. Impact of impregnation composition

Apparently, two different effects influence the water transport behavior in Fig. 10 leading to a maximum water flow. A higher concentration of hydrophobic agent facilitates water removal through the GDL [50] and minimizes liquid water content inside the porous medium [46,51]. In contrast, the capillary transport of liquid water is impeded owing to the enhanced hydrophobicity [19]. Hence, CB possesses a much stronger impact on the gas permeability than the hydrophobic agent owing to its nano-porous structure. Consequently, the tp gas permeability increases linearly with declining CB content resulting in lower mass transport resistance. Furthermore it is assumed that the porous structure of the CB is sealed by the hydrophobic agent when the amount of PTFE is enhanced. However, the correlation between the tp gas permeability and the water transport can only explain the linear slope of the curve in Fig. 10 but can not be held responsible for the reduced water flow when pure PTFE is used for the substrate treatment. In spite of an increased permeability the water flow drops in the absence of CB. Generally, CB is added for two reasons: At first, the fluorinated polymer becomes more homogeneously distributed in the bulk [52] and second, the addition of carbon improves the electrical conductivity of the GDL. Based on the assumption that the hydrophobic agent affects only liquid water but not the water vapor, the presence of liquid water at the GDL/CCM interface could be an explanation for the decay of the water transport rate. If CB is used on the impregnation mixture, liquid water will be able to penetrate into the gas diffusion media due to hydrophilic pathways [41]. Since only PTFE without CB is employed, especially at high loadings, liquid water is blocked at the hydrophobic GDL surface. Even despite a wet-proofing treatment, several authors pointed out a co-existence of both hydrophobic and hydrophilic pores in gas diffusion media [40,53,54]. As a result differences in wettability, e.g. mixed-wettability, occur, which lead to local invasion of liquid water into the material by means of capillary wicking according to the Young–Laplace Eq. (9)

$$p_{H_2O} - p_{air} > p_c = \frac{4\sigma \cos\theta_c}{d_p} \quad (9)$$

Eq. (9) will be satisfied once the liquid water pressure p_{H_2O} at the GDL/CCM interface exceeds the air pressure p_{air} in the GDL pores. Consequently, liquid water invasion occurs with the hydrophilic pores supporting imbibition and hydrophobic pores hindering liquid water transport. According to the Young–Laplace Eq. (9) the required water pressure is defined by the hydrophobicity, e.g. the contact angle and the pore diameter.

Mathias et al. found that the hydrophobic agent distribution in the cross-section of the GDL depends on the drying process [9]. A fast convective drying leads to an inhomogeneous distribution of the hydrophobic agent resulting in a high concentration at the GDL surface whereas a more homogeneous PTFE distribution is observed by means of a slow diffusive drying process. Lim et al. also observed that the hydrophobic agent, i.e. FEP is predominantly located at the GDL surface and clearly reduces porosity as well as enhances the contact angle [30]. Consequently, liquid water becomes inhibited to penetrate into the porous media at the GDL/CCM interface. For exposing this aspect two different drying processes have been compared, a diffusive and a preferably convective drying resulting in dissimilar PTFE distributions. Fig. 10 indicates that the diffusive drying of NW T20h (striped column)

seems to enhance the water transport rate compared to the convectively dried NW T20i. The tp gas permeability of both materials, however, remains at the same level and thus cannot be held responsible for the declined water flow. In conclusion, both the CB content and the amount of PTFE have an impact on the water transport. At high CB/PTFE ratio the mass transport limitation due to the nanoporous CB structure dominates the water removal in the GDL. By increasing the amount of PTFE, mass transport decreases. When a critical level of hydrophobic agent is reached, however, the fluorinated polymer is mainly concentrated at the GDL surface and prevents the invasion of liquid water into the diffusion medium. Latter occurs as soon as the absolute PTFE loading becomes higher than 80%.

4.5. Impact of PTFE distribution

Fig. 11 further emphasizes the observation that the impregnation weight of the substrate influences the water transport behavior in gas diffusion media. The higher the PTFE loading is the worse becomes the water removal. Similar to Fig. 8 an approximately linear correlation is found. In addition, the distribution of the pure hydrophobic agent seems to possess an impact on the water transport, too. Hence, all diffusively dried samples (NW T10h, NW T20h, NW T30h and NW T40h) point to a lower water transport rate than the convectively dried material with corresponding PTFE content (NW T10i, NW T20i, NW T30i and NW T40i) due to a more homogeneous PTFE distribution. The linear decay of the tp permeability, illustrated in the same figure, cannot hold as an explanation for the differences in water transport behavior. Finally, these findings further underline the presence of liquid water at the GDL/CCM interface.

4.6. Impact of temperature

The exponential increase in water transport with increasing temperature (Fig. 12) can be described by means of the Clausius–Clapeyron relation correlating the vapor pressure and the temperature:

$$\frac{\mathrm{d}p}{\mathrm{d}T} = \frac{\Delta_{\mathrm{vap}}H}{\Delta_{\mathrm{vap}}V \cdot T} \tag{10}$$

Eq. (10) can be simplified for ideal gases to

$$\frac{\mathrm{d}p}{p} = \frac{\Delta_{\mathrm{vap}}H}{RT^2}\mathrm{d}T \tag{11}$$

by using $\Delta_{\mathrm{vap}}V \approx V_{\mathrm{mol,g}} = RT/p$ and the assumption that the molar volume of the liquid phase can be neglected compared to the volume of the gas phase. As good approximation the enthalpy of water vapor does not change within the employed temperature range and Eq. (11) is integrated to

$$p_2 = p_1 \exp\left[\frac{\Delta_{\mathrm{vap}}H}{R}\left(\frac{1}{T_2} - \frac{1}{T_1}\right)\right] \tag{12}$$

The exponential correlation in Fig. 12, represented by the samples NW I10-60 and NW I30-60, holds for all investigated materials in the present study and is in accordance with Eq. (12). Hence, these findings emphasize that the water vapor transport (evaporation) plays a crucial role in the water transport measurement. Simple estimations by means of the Magnus formula prove that evaporation is not the limiting process because the speculative saturated water vapor pressure is at least three times larger than the experimentally observed value [55]. Consequently, an equilibrated liquid–vapor two-phase system is present and justifies the use of the Antoine Eq. (7) in Section 2.4. Further, water vapor transport seems to be the predominant transport mechanism in the GDL.

Table 3
Theoretical and experimental diffusion coefficients and water transport rates at 0.6 MPa cell compression (54.5 °C, atm, 15,000 sccm, 50 cm^2)

GDL	NW I20-40 C1
T (°C)	54.5
$D^{\mathrm{air}}_{\mathrm{vap}}$ ($cm^2\ s^{-1}$)	0.293
$D^{\mathrm{air}}_{\mathrm{vap,\,eff}}$ ($cm^2\ s^{-1}$)	0.095
$D^{\mathrm{air}}_{\mathrm{vap}}/D^{\mathrm{air}}_{\mathrm{vap,eff}}$ [a]	3.08
$\dot{m}^{\mathrm{theo}}_{\mathrm{vap}}$ (mg min^{-1})	917
$\dot{m}^{\mathrm{exp}}_{\mathrm{H_2O}}$ (mg min^{-1})	445

[a] Determined according to Baker et al. [44].

4.7. Correlation with diffusive transport

As obvious from Fig. 13 the water transport correlates to the relative diffusivity where a molecular diffusive gas transport driven by a water concentration gradient across the GDL seems to be preferred. Therefore we attempted to determine a theoretical water transport rate based on the system and measurement parameters. The water flow through a GDL can be calculated by means of Fick's law:

$$\dot{n}_{\mathrm{vap}} = -D^{\mathrm{air}}_{\mathrm{vap,eff}}A_{\mathrm{cell}}\frac{\Delta c_{\mathrm{vap}}}{d_{\mathrm{GDL}}} \tag{13}$$

with $\dot{n}_{\mathrm{vap}} = \dot{m}_{\mathrm{vap}}/M_{\mathrm{vap}}$ and $c_{\mathrm{vap}} = n_{\mathrm{vap}}/V_{\mathrm{vap}} = p_{\mathrm{vap}}/RT_{\mathrm{cell}}$ Eq. (14) follows

$$\dot{m}_{\mathrm{vap}} = -D^{\mathrm{air}}_{\mathrm{vap,eff}}A_{\mathrm{cell}}\frac{\Delta p_{\mathrm{vap}}}{d_{\mathrm{GDL}}}\frac{M_{\mathrm{vap}}}{RT_{\mathrm{cell}}} \tag{14}$$

The cell temperature, GDL thickness and the differential partial water vapor pressure can be obtained experimentally whereas the effective diffusion coefficient of water vapor in the GDL can be calculated by means of the experimental relative diffusivity data. Eq. (15) is the consequence

$$\dot{m}_{\mathrm{vap}} = -\frac{D^{\mathrm{air}}_{\mathrm{vap}}}{x}A_{\mathrm{cell}}\frac{\Delta p_{\mathrm{vap}}}{d_{\mathrm{GDL}}}\frac{M_{\mathrm{vap}}}{RT_{\mathrm{cell}}} \tag{15}$$

where $x = D^{\mathrm{air}}_{\mathrm{vap}}/D^{\mathrm{air}}_{\mathrm{vap,eff}}$ is the relative diffusivity. The temperature-dependent diffusion coefficient of water vapor can be estimated via the Fuller–Schettler–Giddings equation [56]:

$$D^{\mathrm{air}}_{\mathrm{vap}} = \frac{0.001T^{1.75}\sqrt{1/M_{\mathrm{air}} + 1/M_{\mathrm{vap}}}}{p\left[\left(\sum v_{\mathrm{air}}\right)^{1/3} + \left(\sum v_{\mathrm{vap}}\right)^{1/3}\right]^2} \tag{16}$$

v_{air} and v_{vap} are the atomic diffusion volume for air and water vapor amounting to 20.1 and 12.7. Both the theoretically calculated and the experimental data of the diffusion coefficients and water transport are summarized in Table 3. Uniform and isotropic diffusion coefficients are used to describe transport phenomena in a simplified manner. Hence, the effective diffusion coefficient $D^{\mathrm{air}}_{\mathrm{vap,eff}}$ of MPL-coated gas diffusion media is an average of the combined diffusion coefficients for the GDL as well as the MPL. Strictly speaking, however, especially in the distinctly smaller MPL pores Knudsen diffusion will occur as well. The presented data in Table 3 indicate that the theoretically calculated water flow is of the same magnitude but twice the experimental rate. Baker et al. introduced a geometrical factor f, which takes the increased diffusion distance under the lands into account to explain deviations of theoretical and experimental values [44]. Therefore water vapor molecules under the lands have to pass a longer diffusion path in order to reach the gas channels instead of flowing through the porous media directly. As a consequence less water can be transported through porous media per time. However, the theoretically calculated mass water transport does not distinguish between the

diffusion distances under land or gas channel resulting in an overestimated water flow rate. Altogether the comparison emphasizes the presumed predominance of diffusive gas transport. In spite of these indications that the molecular gas diffusion probably dominates the water transport in the GDL, we have already mentioned a presumable liquid water transport in the current study as well. Figs. 10 and 11 hint to the fact that the water transport behavior through the gas diffusion media cannot be explained by the gas transport, solely. Furthermore the non-linear correlation between water transport and relative diffusivity in Fig. 13 underlines this supposition, too. If only molecular gas diffusion took place, a linear relationship between both parameters would be observed. Here, we have to remind that a convective transport mechanism and the mass transport resistance by the CCM were neglected.

As it can be seen in Fig. 4 the theoretical water flow is smaller than the experimental one for an air flow below 500 sccm. At these operating conditions the air volume is insufficient to take up the complete liquid water in the GDL. Consequently, water condensates in the GDL as well as in the flow field channels due to a relative humidity higher than 100% on the 'gas side'. When the air flow exceeds 500 sccm the experimental water removal falls below the theoretical one with a relative humidity smaller than 100% at the

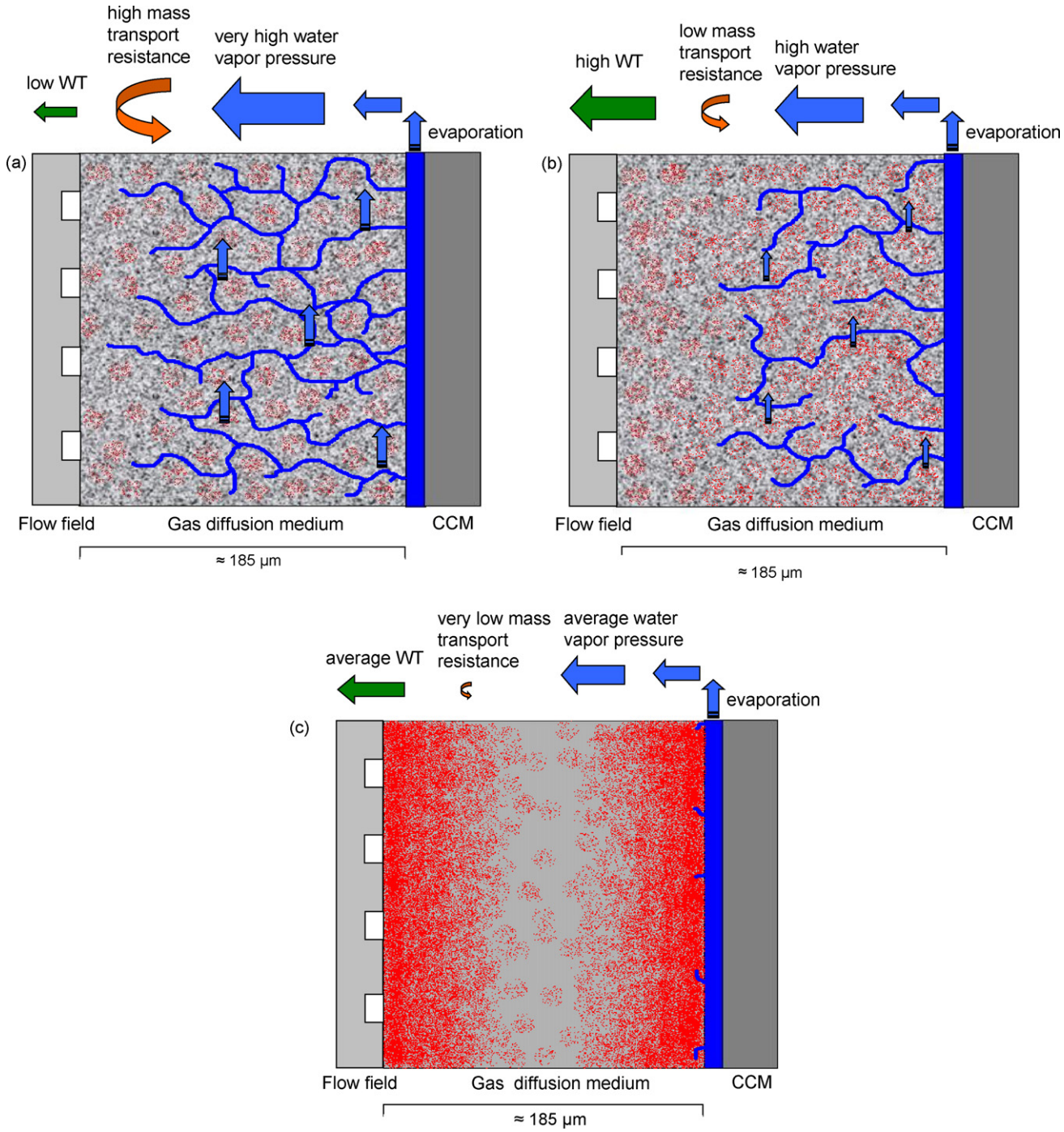

Fig. 14. Water transport model: water transport (WT) through gas diffusion media (a) with high carbon black content, (b) low carbon black content, and (c) only PTFE (no carbon black). (For interpretation of the references to color in the text, the reader is referred to the web version of the article.)

'gas side'. Finally, higher air flow leads to a lower relative humidity owing to the mass transport limitation by the gas diffusion medium. Independent from the investigated material, all WT vs. air flow curves point out a saturated behavior as shown in Fig. 4. Similarly, Wang et al. observed a limitation of heat and mass flux by diffusion media at increased air velocities [42]. A relative humidity below 100%, however, does not exclude liquid water transport into and in the GDL because the relative humidity indicates only an average value of the complete 'gas side', i.e. GDL/CCM interface, GDL and the flow field channels which can be observed experimentally [57].

4.8. Water transport model

As already mentioned in Section 4.6, mass transport (and not evaporation) is the limiting process, which results in a liquid–vapor equilibrium in the water transport system. Based on the experimental results and interpretations a water transport model is proposed which includes both a diffusive water vapor transport and capillary transport of liquid water in the GDL. Thereby, it is assumed that water vapor diffusion is the predominant transport mechanism in the GDL.

The 'gas side' of the test cell is sketched in Fig. 14 and depicts the investigated GDL sandwiched between the CCM and the 'gas side' flow field. In Fig. 14a the non-woven GDL is treated with a very high amount (80%) of CB. Based on above experimental findings it is assumed that there exists liquid water at the GDL/CCM interface, which is able to evaporate and hence, invades easily into the porous medium as gas (blue arrows). Additionally, liquid water can penetrate into the GDL due to hydrophilic pathways (blue). The high CB content (grey) supports the homogeneous distribution of the low PTFE loading (red) in the GDL resulting in a low water pressure, which is necessary to force liquid water into the material according to the Young–Laplace Eq. (9). In addition, the evaporation surface in the GDL increases due to the high specific surface of the carbon. The reduction of both the tp gas permeability and the relative diffusivity in Figs. 9 and 13, respectively, refers to a strong enhancement of mass transport resistance (orange arrow) when the GDL is treated with a high CB loading. Accordingly, the water vapor as well as the liquid water transport becomes inhibited resulting in a low net water transport (green arrow) through the diffusion medium.

In Fig. 14b, the carbon content in the GDL bulk is very low and the hydrophobic agent less homogeneously distributed across the GDL. The PTFE partly migrates to the GDL surface and increases the necessary liquid water pressure for water invasion according to relation (9). Compared to a sample with high CB content (Fig. 14a), a reduced amount of hydrophilic pathways remain at the surface leading to a lower invasion of liquid water in the porous medium. On the other hand the mass transport resistance is clearly reduced due to the low CB loading. Such a sample includes the optimal compromise between low mass transport resistance and sufficient hydrophilic pathways to ensure liquid water invasion into the diffusion medium followed by additional evaporation. In contrast to the aforementioned situation, GDLs treated with a hydrophobic agent only, show lower water removal. The mass transport resistance is minimized as no carbon is included but additional liquid water can not penetrate into the material due to the high PTFE loading at the GDL surface (Fig. 14c) resulting in a lower water transport rate compared to Fig. 14b.

Conclusively, in the presented model the water transport is based on a two-phase mechanism with an important contribution of the evaporation process and gas transport whereas the latter is the limiting process. In general, high impregnation weight as well as an additional MPL prevents the invasion of liquid water flow into the porous substrate. These assumptions are in agreement with Wang et al. where no significant impact of hydrophobicity on the mass transport has been observed and consequently, it was assumed that evaporation and subsequent gas transport is the major transport mechanism instead of capillary transport of liquid water [42].

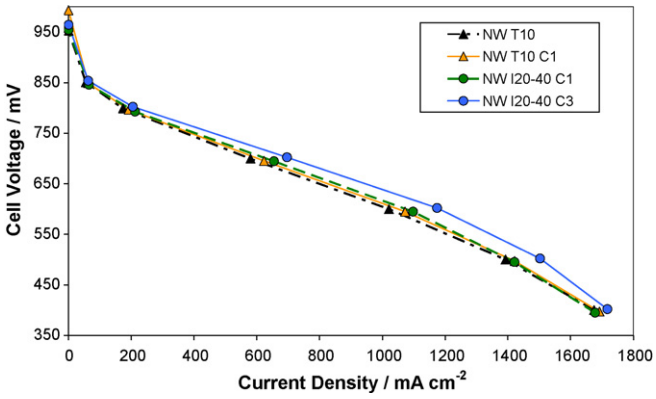

Fig. 15. Polarization curves of different GDLs on dry operating conditions.

4.9. Correlation with in situ performance

In order to correlate *in situ* and *ex situ* findings and prove the proposed model, polarization curves are compared on basis of four carbon fiber non-wovens as presented in Fig. 15. Low humidified conditions were chosen for the *in situ* tests to resemble automotive applications with a relative exit humidity of less than 100%. The same type of GDL was applied at both sides of the electrodes. Moreover, Fig. 16 illustrates the power density at cell voltages of 500 mV, 600 mV, 700 mV and 800 mV (potentiostatic setup) compared with the water transport data. The cell performance tends towards higher values when the mass transport resistance of the GDL is enhanced resulting in lower water transport at all four voltages. NW T10, the material with the lowest loading and no additional MPL, performs the worst, probably due to good removal of product water from the catalyst layer (CL) to the cathode flow field. Consequently, electro-osmotic drag is enforced to exceed back diffusion from the cathode to the anode. As a result the membrane cannot be humidified at the anode sufficiently and low cell performance occurs. In order to explain the best performance of NW I20-40 C3 (20 wt.% CB/PTFE = 60/40, dense hydrophobic MPL), it is assumed that a highly impregnated GDL with an appropriate MPL prevents water removal over the cathode efficiently [36]. Hence,

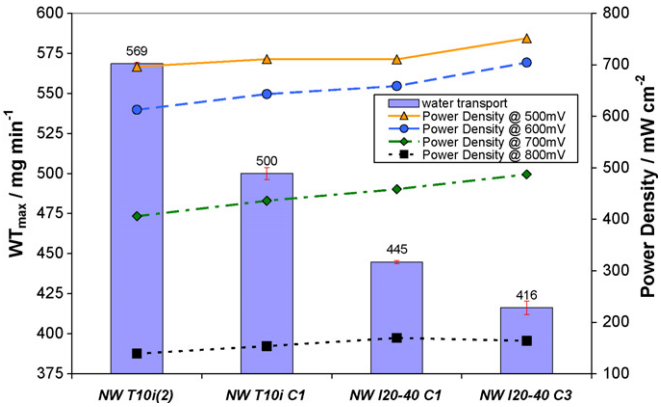

Fig. 16. *Ex situ* water transport measurement (WT) (54.5 °C, atm, 15,000 sccm, 50 cm^2) vs. *in situ* performance on dry operating conditions.

back diffusion to the anode is delivered and membrane dehydration at the anode can be inhibited resulting in a reduced performance loss due to ohmic resistance [12,58].

Thus, these first correlations show that a MPL on the GDL as well as an alternative hydrophobic impregnation of the gas diffusion medium substrate improves the *in situ* performance [19]. Further these findings are able to validate the experimental measurements of water transport in gas diffusion media. As mentioned above dry operating conditions were used which do not allow an extrapolation on wet conditions. The cell performance can be presumably enhanced further when two different GDL types are used at the electrodes (asymmetric setup) to achieve the most efficient water management in the cell

5. Conclusions

A new *ex situ* test method was developed for evaluating gas diffusion media in terms of water transport. Increased GDL thickness significantly reduces water flow due to the longer diffusion pathways. Mass transport resistance increases by an additional MPL on the porous substrate and enhanced impregnation weight, respectively. The water removal rate can be reduced by a small CB/PTFE impregnation ratio as well. Further an inhomogeneously distributed pure PTFE treatment without additional carbon blocks the liquid water intrusion at the GDL/CCM interface and lowers the water transport. In addition the water transport rate shows an exponential dependence on the cell temperature. Based on these findings a two-phase water transport model has been proposed which assumes diffusive gas as well as liquid water transport in diffusion media in which the gas phase is predominant. Good correlations between experimental *ex situ* data and *in situ* performance at elevated temperature in PEMFCs were found on low humidified conditions. Based on the experimental results guidelines can be given towards new design concepts for gas diffusion media regarding optimized water management.

Acknowledgement

The authors would like to thank the International Technical Development Center of the Adam Opel AG in Rüsselsheim (Germany) for implementing the gas diffusion measurements.

References

[1] D.P. Wilkinson, H.H. Voss, K. Prater, J. Power Sources 49 (1994) 117–127.
[2] T.A. Zawodzinski, C. Derouin, S. Radzinski, R.J. Sherman, T. van Smith, T.E. Springer, S. Gottesfeld, J. Electrochem. Soc. 140 (1993) 1041–1047.
[3] P. Berg, K. Promislow, J. St-Pierre, J. Stumper, B. Wetton, J. Electrochem. Soc. 151 (2004) A341–A353.
[4] M. Watanabe, Y. Satoh, C. Shimura, J. Electrochem. Soc. 140 (1993) 3190–3193.
[5] J.G. Pharoah, K. Karan, W. Sun, J. Power Sources 161 (2006) 214–224.
[6] G. Lin, W. He, T.V. Nguyen, J. Electrochem. Soc. 151 (2004) A1999–A2006.
[7] D. Natarajan, T.V. Nguyen, AIChE J. 46 (2000) 2053–2064.
[8] P. Staiti, Z. Poltarzewski, V. Alderucci, G. Maggio, N. Giordano, A. Fasulo, J. Appl. Electrochem. 22 (1992) 663–667.
[9] M.F. Mathias, J. Roth, J. Fleming, W. Lehnert, in: W. Vielstich, A. Lamm, H.A. Gasteiger (Eds.), Handbook of Fuel Cells—Fundamentals, Technology and Applications, vol. 3, John Wiley & Sons, New York, 2003, pp. 517–537.
[10] J. Larminie, A. Dicks, Fuel Cell Systems Explained, John Wiley & Sons, 2000.
[11] D. Bevers, R. Rogers, M. Von Bradke, J. Power Sources 63 (2) (1996) 193–201.
[12] G. Lin, T.V. Nguyen, J. Electrochem. Soc. 152 (10) (2005) A1942–A1948.
[13] T. Zawodzinski, J. Bauman, F. Urbe, S. Gottesfeld, E.S. DeCastro, M. DeMarinis, in: S. Gottesfeld, T.F. Fuller (Eds.), Proceedings of the Second International Symposium on Proton Conducting Membrane Fuel Cells, Pennington, NJ, Electrochem. Soc. (1999) 1.
[14] M.V. Williams, H.R. Kunz, J.M. Fenton, J. Power Sources 135 (2004) 122–134.
[15] S. Escribano, J.F. Blachot, J. Etheve, A. Morin, R. Mosdale, J. Power Sources 156 (2006) 8–13.
[16] T.R. Ralph, G.A. Hards, J.E. Keating, S.A. Campbell, D.P. Wilkinson, M. Davis, J. St-Pierre, M.C. Johnson, J. Electrochem. Soc. 144 (11) (1997) 3845–3857.
[17] T. Frey, M. Linardi, Electrochim. Acta 50 (1) (2004) 99–105.
[18] M.V. Williams, E. Begg, L. Bonville, H.R. Kunz, J.M. Fenton, J. Electrochem. Soc. 151 (2004) A1173–A1180.
[19] G.G. Park, Y.J. Sohn, T.H. Yang, Y.G. Yoon, W.Y. Lee, C.S. Kim, J. Power Sources 131 (2004) 182–187.
[20] E.R. Gonzalez, S. Srinivasan, Int. J. Hydrogen Energy 9 (1984) 215–218.
[21] Fuel Cell Handbook, 6th ed., Washington, DC, U.S. Dept. of Energy, 2002, DOE/NETL-2002/1179.
[22] J.T. Gostick, M.W. Fowler, M.A. Ioannidis, M.D. Pritzker, Y.M. Volfkovich, A. Sakars, J. Power Sources 156 (2006) 375–387.
[23] H.K. Atiyeh, K. Karan, B. Peppley, A. Phoenix, E. Halliop, J. Pharoah, J. Power Sources 170 (2007) 111–121.
[24] M. Prasanna, H.Y. Ha, E.A. Cho, S.A. Hong, I.H. Oh, J. Power Sources 131 (2004) 147–154.
[25] B. Thoben, A. Siebke, J. New Mater. Electrochem. Syst. 7 (2004) 13–20.
[26] Z. Qi, A. Kaufman, J. Power Sources 109 (2002) 38–46.
[27] D.P. Wilkinson, J. St.-Pierre, in: W. Vielstich, A. Lamm, H.A. Gasteiger (Eds.), Handbook of Fuel Cells—Fundamentals, Technology and Applications, vol. 3, John Wiley & Sons Ltd., New York, 2003, pp. 609–626.
[28] L. Giorgi, E. Antolini, A. Prozio, E. Passacqua, Electrochim. Acta 43 (1998) 3675–3680.
[29] J. Moreira, A.L. Ocampo, P.J. Sebastian, M.A. Smith, M.D. Salazar, P. Del Angel, J.A. Montoya, R. Pérez, L. Martínez, Int. J. Hydrogen Energy 28 (2003) 625–627.
[30] C. Lim, C.Y. Wang, Electrochim. Acta 49 (2004) 4149–4156.
[31] F. Lufrano, E. Passalacqua, G. Squadrito, A. Patti, L. Giorgi, J. Appl. Electrochem. 29 (1999) 445–448.
[32] S. Park, J.-W. Lee, B.N. Popov, J. Power Sources 163 (2006) 357–363.
[33] L.R. Jordan, A.K. Shukla, T. Behrsing, N.R. Avery, B.C. Muddle, M. Forsyth, J. Power Sources 86 (2000) 250–254.
[34] V.A. Paganin, E.A. Ticianelli, E.R. Gonzalez, J. Appl. Electrochem. 26 (1996) 297–304.
[35] J. Yu, Y. Yoshikawa, T. Matsuura, N. Islam, M. Hori, Electrochem. Solid-State Lett. 8 (3) (2005) A152–A155.
[36] U. Pasaogullari, C.Y. Wang, Electrochim. Acta 49 (2004) 4359–4369.
[37] A.Z. Weber, J. Newman, J. Electrochem. Soc. 152 (2005) A677–A688.
[38] G. Lin, T.V. Nguyen, J. Electrochem. Soc. 153 (2006) A372–A382.
[39] U. Pasaogullari, C.Y. Wang, K.S. Chen, J. Electrochem. Soc. 152 (2005) A1574–A1582.
[40] J.H. Nam, M. Kaviany, Int. J. Heat Mass Transf. 46 (2003) 4595–4611.
[41] X.G. Wang, F.Y. Zhang, A.L. Lubawy, C.Y. Wang, Electrochem. Solid-State Lett. 7 (2004) A408–A411.
[42] S. Wang, Y. Utaka, Y. Tasaki, Heat Transf. Asian Res. 35 (2) (2006) 137–151.
[43] H.D. Baehr, Thermodynamik, 8th ed., Springer-Verlag, Berlin/Heidelberg/New York, 1994.
[44] D. Baker, C. Wieser, K.C. Neyerlin, M.W. Murphy, ECS Trans. 3 (2006) 989–999.
[45] J.H. Jang, W.M. Yan, C.C. Shih, J. Power Sources 156 (2006) 244–252.
[46] E.C. Kumbur, K.V. Sharp, M.M. Mench, J. Power Sources 168 (2007) 356–368.
[47] Z. Zhan, J. Xiao, D. Li, M. Pan, R. Yuan, J. Power Sources 160 (2006) 1041–1048.
[48] R. Flückiger, S. Freunberger, D. Kramer, G.G. Scherer, A. Wokaun, F.N. Büchi, PSI Electrochemistry Laboratory Annual Report, 2006.
[49] B. Mueller, T. Zawodzinski, J. Baumann, F. Uribe, S. Gottesfeld, in: S. Gottesfeld, T.F. Fuller (Eds.), Proton conducting Membrane Fuel Cells II, Proceedings, vol. 98–27, The Electrochemical Society Proceedings Series, Pennington, NJ, 1998, p. 1.
[50] E.C. Kumbur, K.V. Sharp, M.M. Mench, J. Power Sources 161 (2006) 333–345.
[51] M. Gan, L.D. Chen, in: The 4th International Conference on Fuel Cell Science, Eng. Technol. (2006).
[52] Y.W. Chen-Yang, T.F. Hung, J. Huang, F.L. Yang, J. Power Sources 173 (2007) 183–188.
[53] G. He, Z. Zhao, P. Ming, A. Abuliti, C. Yin, J. Power Sources 163 (2007) 846–852.
[54] P.K. Sinha, P.P. Mukherjee, C.Y. Wang, J. Mater. Chem. 17 (2007) 3089–3103.
[55] D. Sonntag, D. Heinze, Sättigungsdampfdruck- und Sättigungsdampfdichtetafeln für Wasser und Eis, 1st ed., VEB Deutscher Verlag für Grundstoffindustrie, 1982.
[56] E.N. Fuller, P.D. Schettler, J.C. Giddings, Ind. Eng. Chem. 58 (5) (1966) 19–27.
[57] I. Manke, C. Hartnig, M. Grünerbel, W. Lehnert, N. Kardjilov, A. Haibel, A. Hilger, J. Banhart, H. Riesemeier, Appl. Phys. Lett. 90 (2007) 174105.
[58] S. Vengatesan, H.J. Kim, E.A. Cho, S.U. Jeong, H.Y. Ha, I.H. Oh, S.A. Hong, T.H. Lim, J. Power Sources 156 (2006) 294–299.